New Sector Scan Geometry for High Frame Rate 2D-Echocardiography using Phased Arrays

Wided Hechkel[1], Néjib Hassen[3]
Laboratory uEI
University of Monastir
Monastir, Tunisia

Brahim Maaref[2]
Laboratory EuE
University of Monastir
Monastir, Tunisia

***Abstract*—2D echocardiography high frame rate techniques do have some drawbacks such as crosstalk artifacts caused by the interactions between the parallel transmitted and received beams. In this paper, we suggest a new cardiac imaging technique based on MLT (Multi-Line Transmission). The main idea of our approach is to benefit from the scan geometry to reduce the interference between the simultaneously transmitted beams. We propose to do the scan at different depths and in parallel to the diagonal scan sector. Therefore, compared to existing MLT techniques, the new scan sector strategy will result in artifacts' reduction in the ultrasound imaging systems. We entitled our approach the Synthetic Sum of Multi-Line Transmission (SS-MLT). Simulations of Point Spread Function (PSF), multiple Point Spread Functions (PSFs) and Cyst Phantom (CP) provided in this paper are compared in our approach to the main classical ultrasound imaging approaches. Therefore, the SS-MLT exhibits a very similar lateral profile as the Single Line Transmission (SLT) algorithm. Hence, the simulation results indicate a potential value of a future hardware implementation of SS-MLT technique.**

***Keywords*—2D Echocardiography; high frame rate; multi-line transmit beamforming; new scan geometry; reduced crosstalk**

I. Introduction

The most critical challenge with the 2D echocardiography is to operate at a high temporal resolution without adversely affecting the image quality of the system. A higher frame rate may allow a more precise recognition of the overall cardiac morphology and its mechanical events. In diagnostic ultrasound imaging systems, the frame rate relies essentially on three parameters; speed of sound over the tissue, penetration depth and the number of events' transmission per frame.

Many researches were about increasing the frame rate by decreasing the number of transmit events for one frame. Among these researches we mention Diverging Wave (DW) imaging [1,2], Multiline Acquisition (MLA) [3,4] and Multiline Transmission (MLT) [5-9]. All these methods operate at an increasing temporal resolution compared to the conventional cardiac imaging techniques. They tried to come up with solutions that give a good tradeoff between image quality and high frame rate. But all the ultrafast techniques mentioned above relatively cause a loss in Signal to Noise Ratio (SNR).

The most used method is the MLT which involves transmitting multiple ultrasonic beams simultaneously with a gain in frame rate similar to the amount of parallel emissions [10–19]. The fundamental concept beyond the MLT technique is a parallel transmission of several focused pulses in different directions, separated by a static opening angle.

But, the problem of this method is the crosstalk artifacts generated by interference on transmission and reception [8] - [13]–[18]. Many researches focused on solving these problems, one possibly with the use of changed frequency ranges for every sent pulse [19]–[20], the adoption of the approaches namely pulse inversion to erase the influences of the extra insonified trends [21] or control the windowing weights of the emitted and acquired signals in order to conform the orientation of the main lobes of the concerned waves, to the orientation of the zeros in the sidelobe fields of the extra waves [22].In [23],the given authors propose a simultaneous multi-zone focusing method using orthogonal quadratic chirp signals to improve the lateral resolution without sacrificing the frame rate. In the proposed method, two weighted quadratic chirp signals with different spectra are simultaneously transmitted with different transmission time delays for a multi-zone focusing. Because the two weighted quadratic chirps can be designed to have a desired level of cross-correlation after compression, the degradation of axial resolution resulting from the division of a spectrum is minimized. In [24], the given authors suggest using the Second-Harmonic Signal in MLT. Therefore, taking advantage of the nonlinear propagation of sound within the tissue, the second-harmonic signal can be used with the MLT technique. The image obtained using the second-harmonic signal, compared to an image obtained by using the fundamental signal, should have reduced artifacts coming from other pulses transmitted simultaneously. In [25] coded excitation has been put forward for crosstalk suppression.

Inappropriately, no one of these techniques has shown an effective suppression of the crosstalk artifacts without affecting the spatial resolution of the output image. Also, most of them exhibit a high circuitry complexity and require a very difficult implementation.

We bring to the fore a new solution based on the geometries that take advantage of three main mechanisms. First, our method uses the MLT approach to form 9 LRIs (Low Resolution Images) and combines them to reconstruct one HRI (High Resolution Image). Second, it adopts a sparse aperture in transmission to avoid interference between adjacent beams, where each of the apertures is connected to an

appropriate pulse generator. Third, the focusing points for simultaneous transmission beams are split diagonally in parallel to the diagonal scan sector, which can dramatically decrease the crosstalks in the image. Using this approach, we maintain a frame rate of about 570 HZ allowing 2-D echocardiographic applications.

In this paper, our objective is to demonstrate that our proposed method can minimize the interference dramatically between transmission/reception pressure fields. Simulations' results of the PSF (Point Spread Function) and CP (Cyst Phantom) prove that this method reduces the production of undesirable artifacts and produces an image quality (IQ) comparable to the IQ of the DRF algorithm.

The following section explains the theroretical background of the different crosstalks in the MLT. Section III presents the new approach for a full MLT sector scan geometry for 2d echocardiography. Simulation results for PSF (Point Spread Function) and CP (Cyst Phantom) are presented in Section IV. Section V discusses SS-MLT technique results in comparison with other algorithms. The inferences and conclusions along with the future scope of study is presented in Section VI.

II. Theoretical Background: MLT-MLA

MLT algorithm is subject to the crosstalk artifacts generated by the interference between beams on transmission and on reception [8] - [13] - [18]. These crosstalks can be classified into three types [13]: transmission crosstalk, reception crosstalk, and transmission/reception crosstalk.

A. Transmission Crosstalk

In this section, we explain how and why the transmission crosstalks between all the ultrasound pressure fields appear in the system. Fig. 1 illustrates the overall transmission crosstalk process in the case of 8-MLT where eight simultaneous beams' focus are at the same depth, but at different angles. The given figure highlights the interactions between the fourth and fifth regions' targets. These communications are the same for all adjacent transmission directions.

We notice an overlapping between the side lobes of the transmission line and the main lobe of the adjacent reception lines steered in a changed orientation. Hence, the side lobe energy of the first transmission beam is picked up by the main lobe of the second reception beam. The number of crosstalks is important under these circumstances.

Transmission crosstalk generates a perturbation that affects measured data with spurious patterns. It is due to the energy transmitted outside the steering direction. The principle three causes of transmission crosstalk are as follows: first the small angular separation between the simultaneously transmitted beams. Second, the less directive beam with high sidelobe levels is also responsible for increasing those perturbations. Third, the same focusing depth shared between all parallel transmission lines is a dramatic factor that produces crosstalks, and this is explained whenever an array element receives a signal that is not reflected from its intended target but generated by neighbour elements and picked up with its own generated signals at the same time.

B. Reception Crosstalk

Fig. 2 illustrates the reception crosstalks in the system. The ultrasound pressure fields mentioned in the figure are measured under the same conditions as transmission crosstalk; focusing at the same depth with 8MLT and each line is insonified from one sub-aperture. We can easily remark an overlapping between the main lobe of the transmission line and the side lobes of the adjacent reception lines steered in a changed orientation. Hence, the main lobe energy of the first transmission beam is picked up by the side lobe of the second reception beam. Also, here, the number of crosstalks is significantly important.

Reception crosstalk produces an interference leading to a high noise in the detected patterns. This noise is due to the effect of echoes coming from scatterers that are not situated in the direction of interest. Like transmission crosstalk, the central causes of reception crosstalk are the small angular separation between the parallel transmitted lines, the ignore of using an apodization to the aperture at reception and, applying the same focusing depth to all parallel transmit directions that generates conjunction in time between transmit and receive fields.

C. Transmision / Reception Crosstalk

Fig. 3 demonstrates the transmission/reception crosstalks in the system. The ultrasound pressure fields mentioned in the aforementioned figure are taken under the same depth with 8MLT and each line is insonified from one sub-aperture. We notice an overlapping between the side lobes of the transmission line and the side lobes of the adjacent reception lines steered in a changed orientation. Hence, the side lobe energy of the first transmission beam is picked up by the side lobe of the second reception beam. Hence, the crosstalks' density is increased under these conditions appear like parasitic blocks in the ultrasound image. This type of crosstalks has the same causes of appearing like transmission crosstalk and reception crosstalk. Hence, the non-adoption of apodization windows in transmission and reception, the thin separating angle between transmission directions, both with the conjunction in time between reception and transmission signals all help this crosstalks' type to appear.

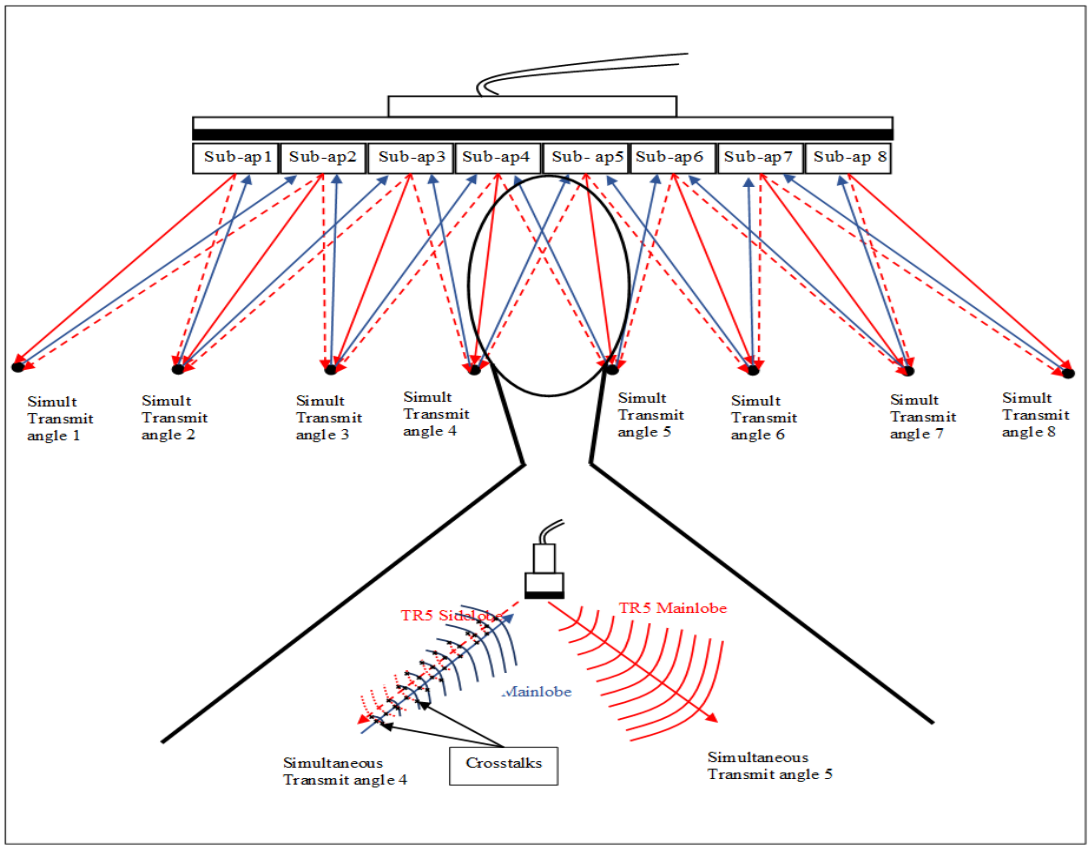

Fig. 1. Illustration of Transmission Crosstalk for same Focusing Depths.

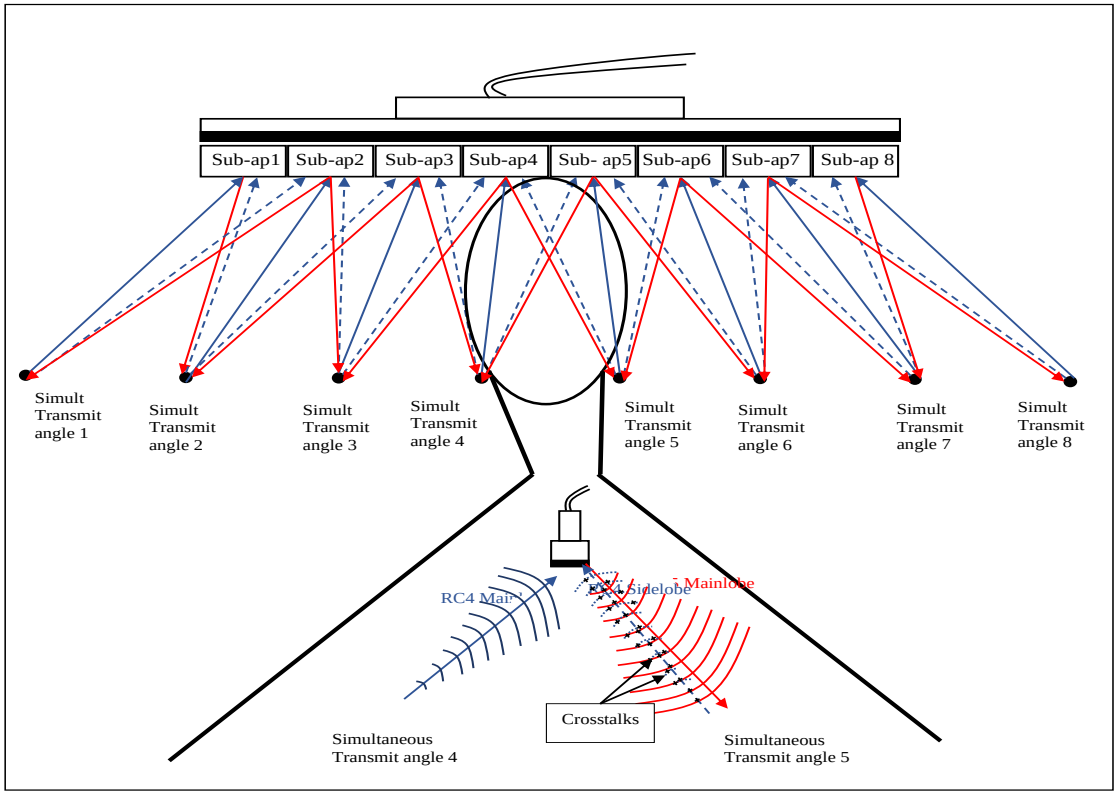

Fig. 2. Illustration of Reception Crosstalk for the same Focusing Depths.

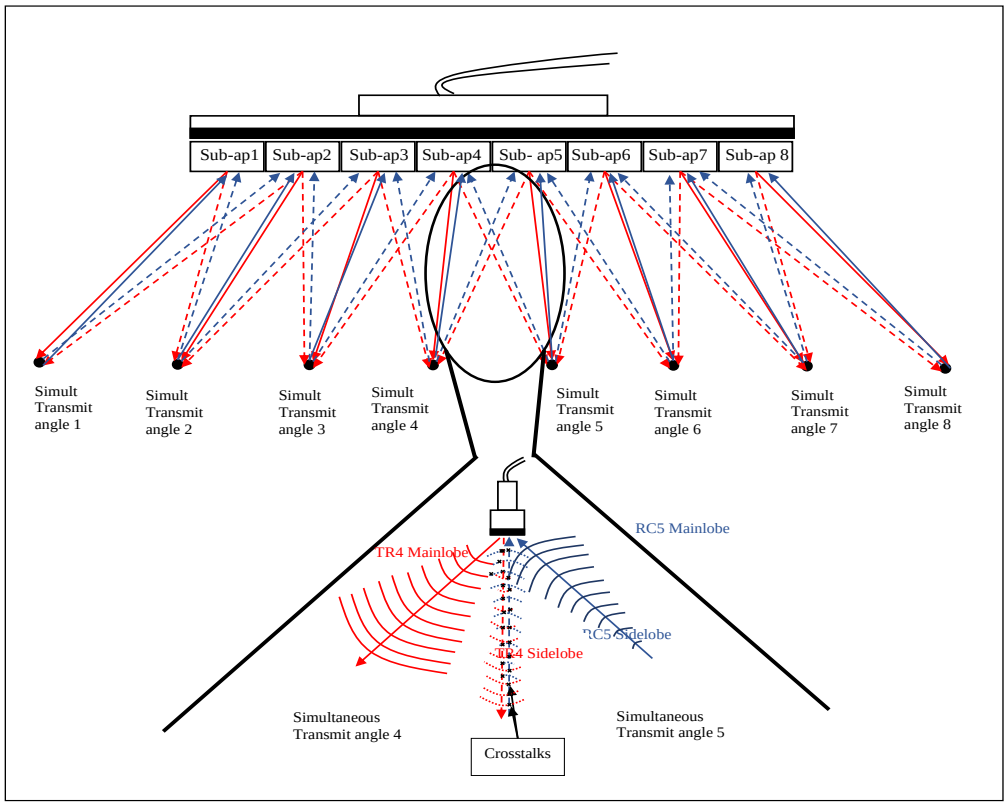

Fig. 3. Illustration of Transmission / Reception Crosstalk for the same Focusing Depths.

III. A New Approach for a Full MLT Sector Scan Geometry for 2D Echocardiography

A. Proposed Algorithm

In this work, we propose to benefit from the sector scan geometry to drastically reduce the crosstalk in the MLT technique. We talk about Synthetic Sum of full MLT (SS-MLT) low resolution images' algorithm. The four main ideas of our proposed algorithm are:

- Focusing at different depths in the same transmission event to considerably reduce main lobe crosstalk between two adjacent transmission lines. In other words, every transmission line focuses on the specific depth where the focusing points formed a diagonal line parallel to the diagonal direction of the sector scan image. Fig. 4 Illustrates Transmission Crosstalk reduction when each transmission sub-aperture focuses at different depths from other sub-apertures. We observe that the friction between the transmission side's lobe of TR5 and the reception of the main lobe of an adjacent RC4 is decreased. Also, the side lobe of the transmission direction is approaching to its original direction, so the distance between this one and the reception field of the adjacent focusing line is broadened. The restrained contact between the transmission side lobe and the reception of the main lobe results in a dramatic reduction of the transmission crosstalks compared to the traditional MLT algorithm.

Fig. 5 Shows Reception Crosstalk's reduction using this process, we notice that the contact between the transmission main lobe of TR5 and reception side lobe of adjacent RC4 line is reduced. Also, we note that the angles of emissions are broadened because the side lobe of the reception direction is approaching to its original one. Because of these two reasons, the reception crosstalk possibility in the system is highly limited compared to reception crosstalk possibility in the same focusing depth emission.

Fig. 6 presents the explanation of transmission/Reception Crosstalk reduction with simultaneous transmissions focusing at different depths. We remark that the contact between the transmission side lobe of one line and the reception side lobe of an adjacent line is reduced. Also, we note that the angle between the two sidelobes is broadened because each side lobe is getting close to its original direction, and the angle between the main transmission lobe and the main reception one of adjacent fields is widened. All this makes transmission/reception crosstalks at its minimum level.

- Using sparse emitting sub-apertures, to avoid sidelobe interference between adjacent, synchronous and transmitted waves relative to each transmitted beam. Each sub-aperture is apodized with Hanning apodization as it is presented in Fig. 7. Fig. 8 combines focuses at different depths and sparse emitting subapertures that have as consequence a very tiny transmission/reception crosstalks. Therefore, sparse emission leads to a more widened angle between adjacent fields. We observe that the main lobe reception and adjacent transmission side lobe are spaced enough

so that there is almost no overlap between them, and the crosstalks are almost eliminated. Fig. 9 demonstrates the same result of a further reduction of reception crosstalk. Hence, the transmission main lobe and the adjacent reception side lobe are very spaced. Also, a very important reduction in transmission/reception crosstalks is observed in Fig. 10.

- Maintaining a high image power by focusing, several times, on different depths at the same zone, so that we disturb energy at all the sectors' scan geometry. Here, after each transmission event, we obtain one low-resolution image. After the summation of all the low-resolution images, we construct one high-resolution image which is the result of focusing on the morphological geometry (Fig. 11).
- Maintaining a high frame rate: For creating a cardiac imaging system, we must work at an increased frame rate specification. Analytically, one transmission/reception event takes about 200 us for a penetration depth of 15 cm and a speed of sound of 1540 m-s . Thereby, to maintain a 300 Hz frame rate, we are limited by 17 transmission-reception events. We divide the sector scan into 8 zones and insonifying each zone with sparse sub-apertures twice.

B. Scan Zones' Division

The most common causes of artifacts through MLT are the transmission and reception crosstalks; an immediate outcome of the communication between each main lobe line and the extra waves side lobes. We can easily observe that main-lobe/side- communications between adjacent transmitted lines can be reduced when we set each focus point of each transmission line at a different depth from the other adjacent focus points.

An accurate decision is to disturb the various focusing points along the line that is parallel to one of the diagonals of the scan geometry sector, as represented in Fig. 12. We obtain 8 scan zones. Different zones can have different numbers of focusing points. The intersection between scan lines and diagonals forms a sub-scan zone. In each sub-zone we have a focus point.

C. Insonification Table

We perform two insonifications to form one zone imaging. After the two transmission /reception events, we construct one low-resolution image. When performing 16 transmission/reception events, we obtain 8 low-resolution images. These images are summed together to put a high-resolution image.

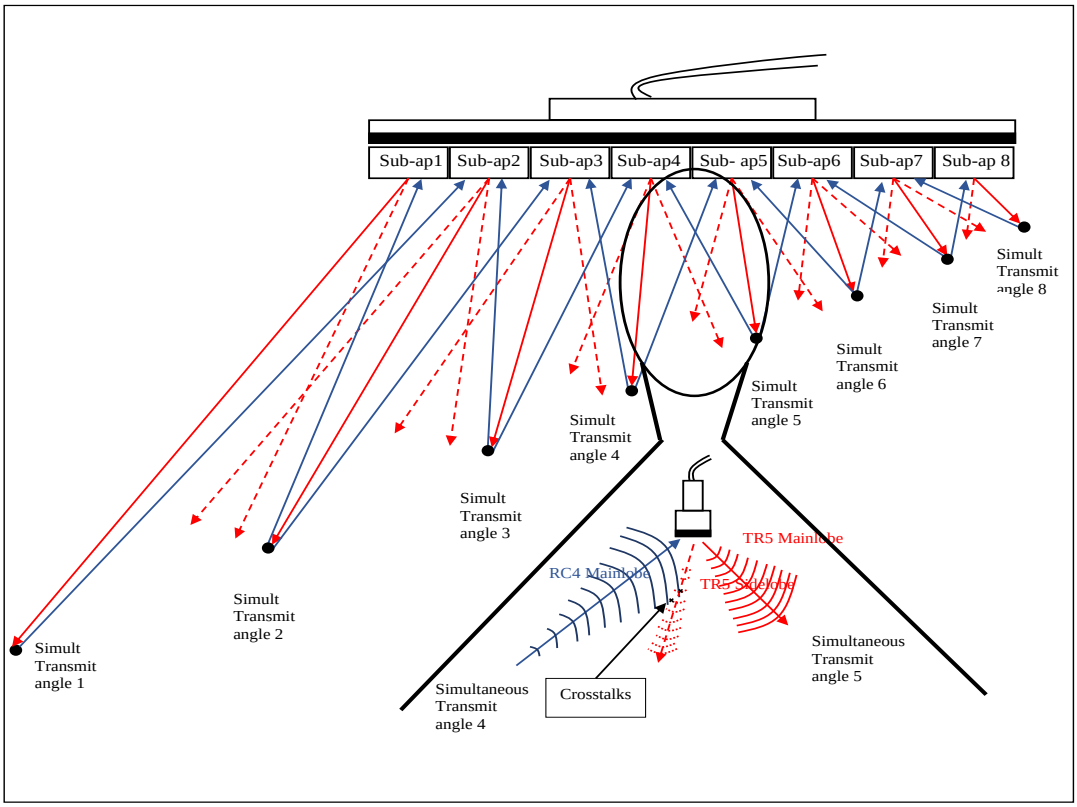

Fig. 4. Illustration of Transmission Crosstalk Reduction for different Focusing Depths.

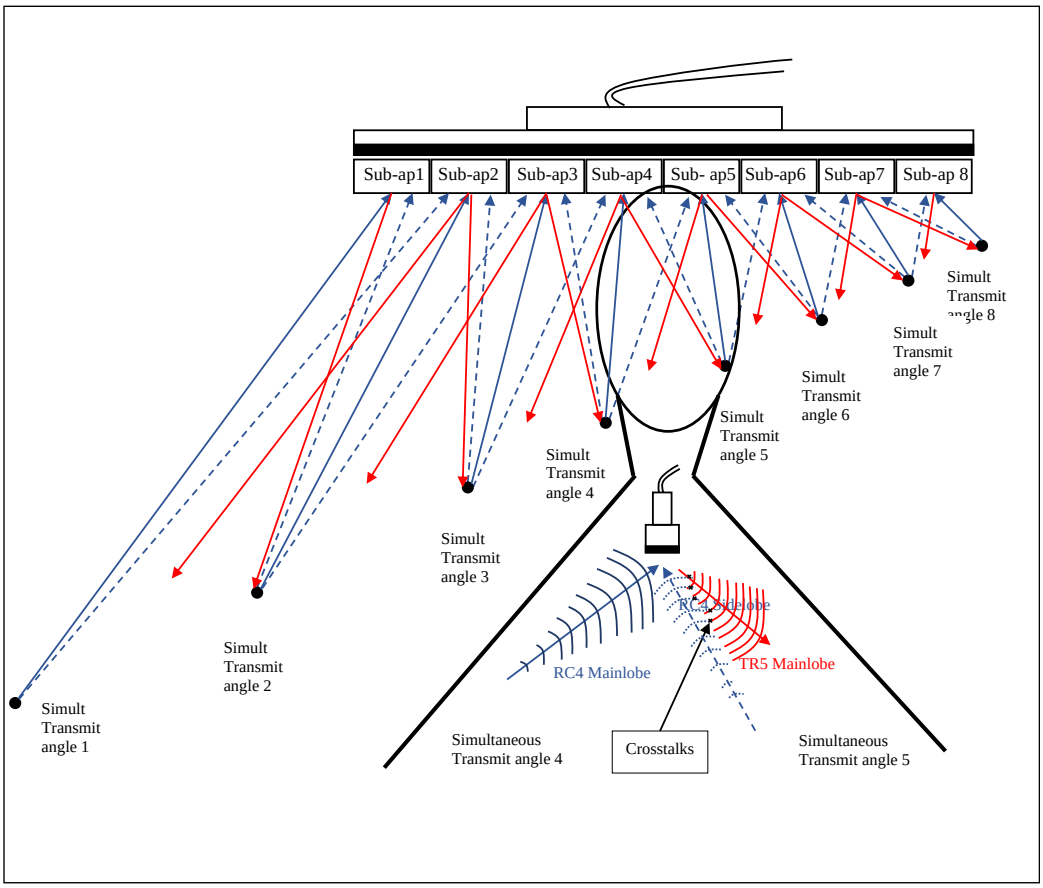

Fig. 5. Illustration of Reception Crosstalk Reduction for different Focusing Depths.

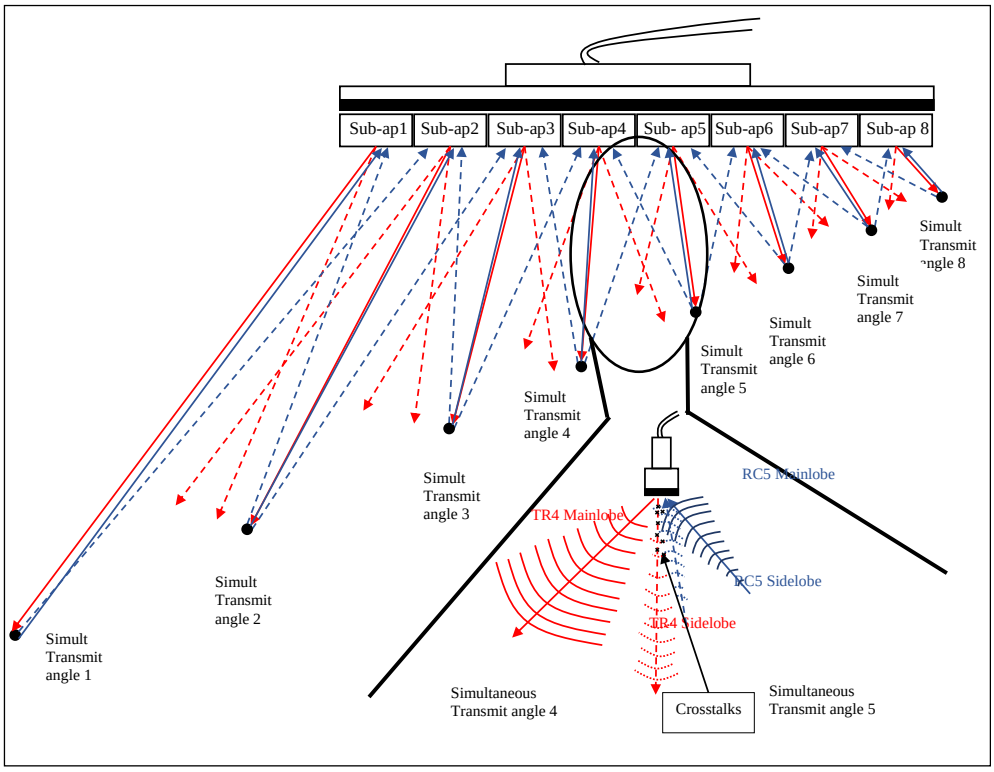

Fig. 6. Illustration of Transmission / Reception Crosstalk Reduction for different Focusing Depths.

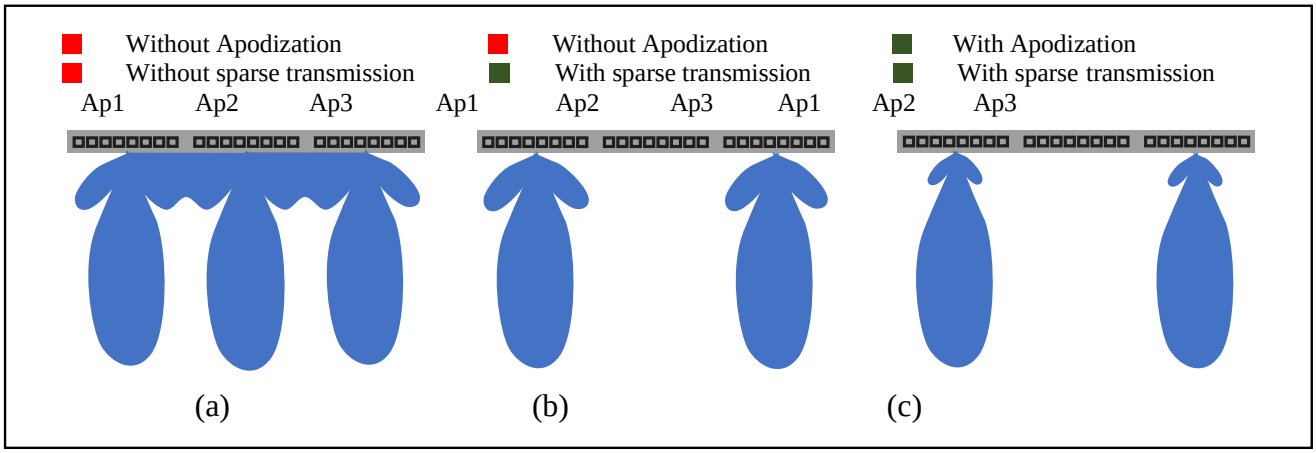

Fig. 7. Sidelobe Interference Reduction Steps (a) Sidelobe Interference Scheme before Apodization and without Sparse Transmission (b) Sidelobe Scheme before Apodization and after Sparse Transmission (c) Sidelobe Reduction Scheme after Apodization and after Sparse Transmission.

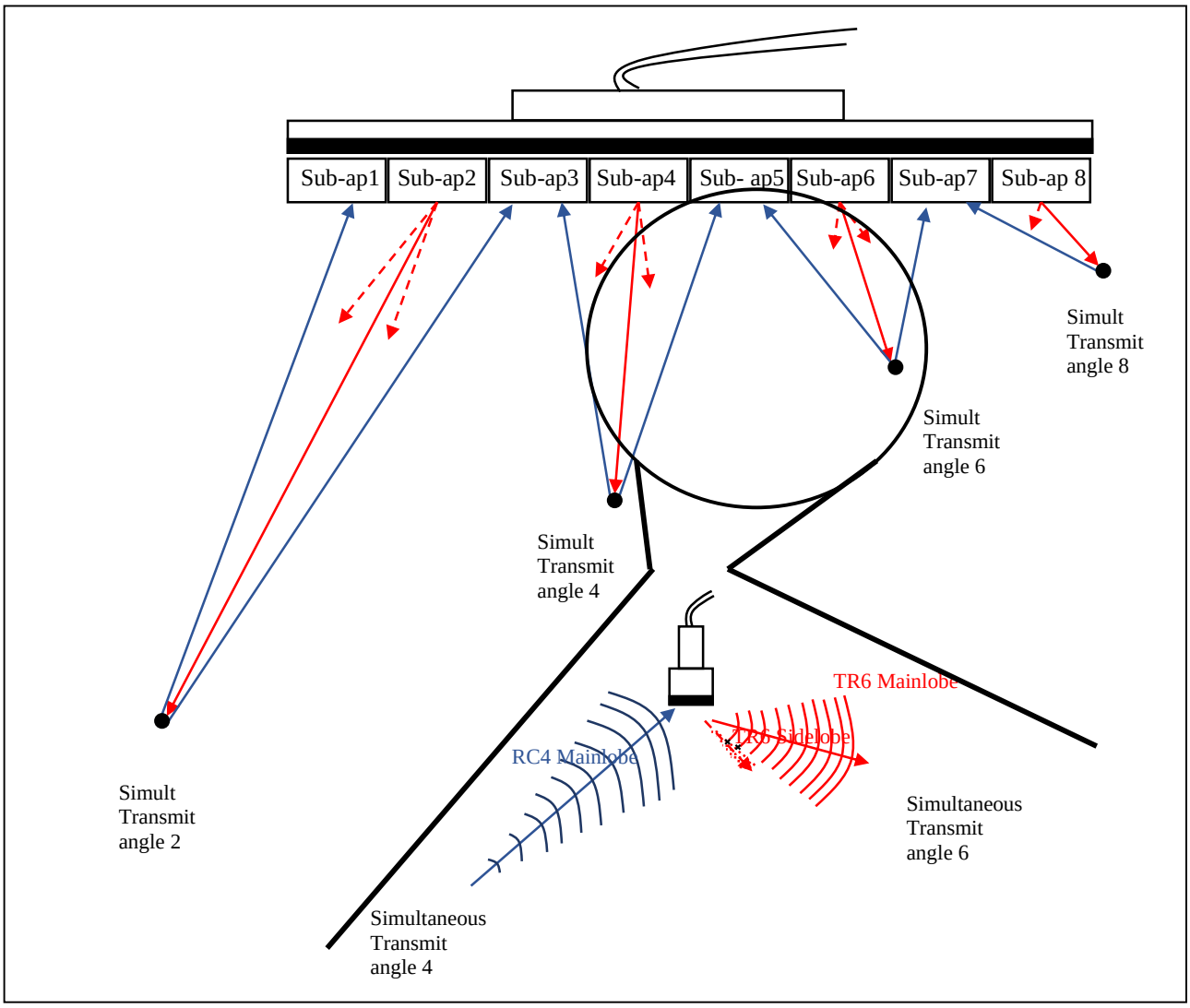

Fig. 8. Illustration of Transmission Crosstalk Reduction for different Focusing Depths and with Sparse Emitting Sub-apertures.

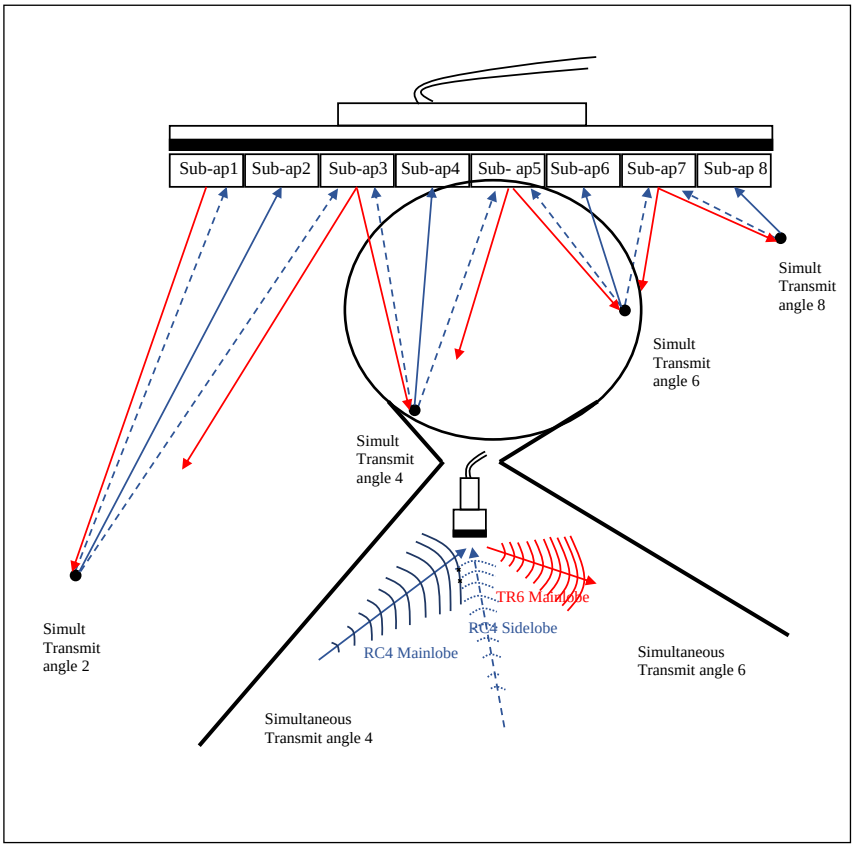

Fig. 9. Illustration of Reception Crosstalk Reduction for different Focusing Depths and with Sparse Emitting Sub-apertures.

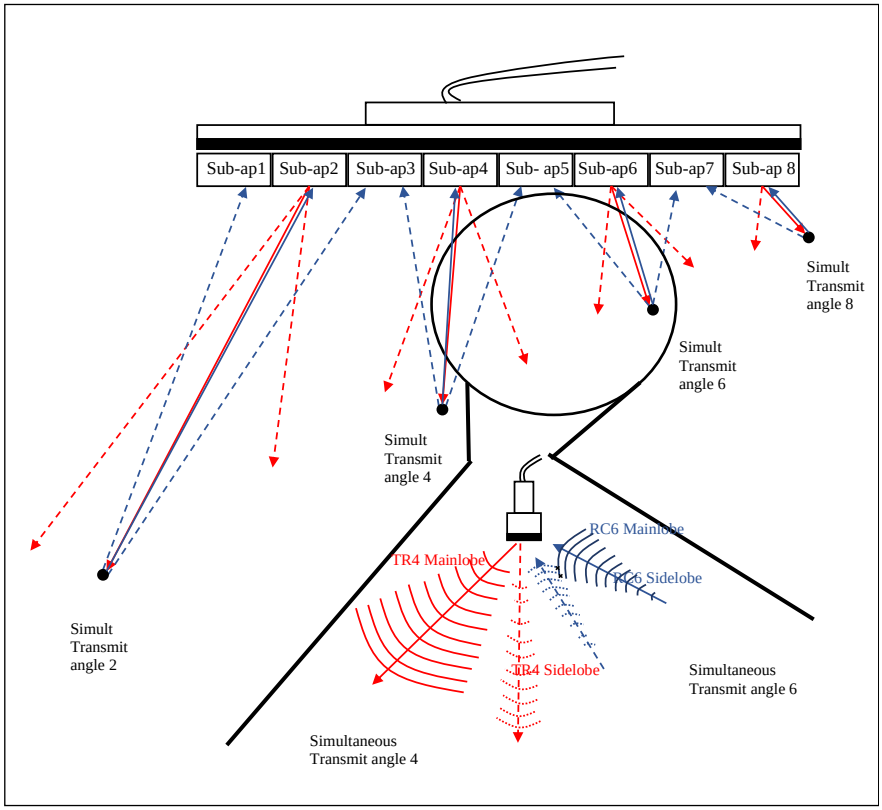

Fig. 10. Illustration of Transmission / Reception Crosstalk Reduction for different Focusing Depths and with Sparse Emitting Sub-apertures.

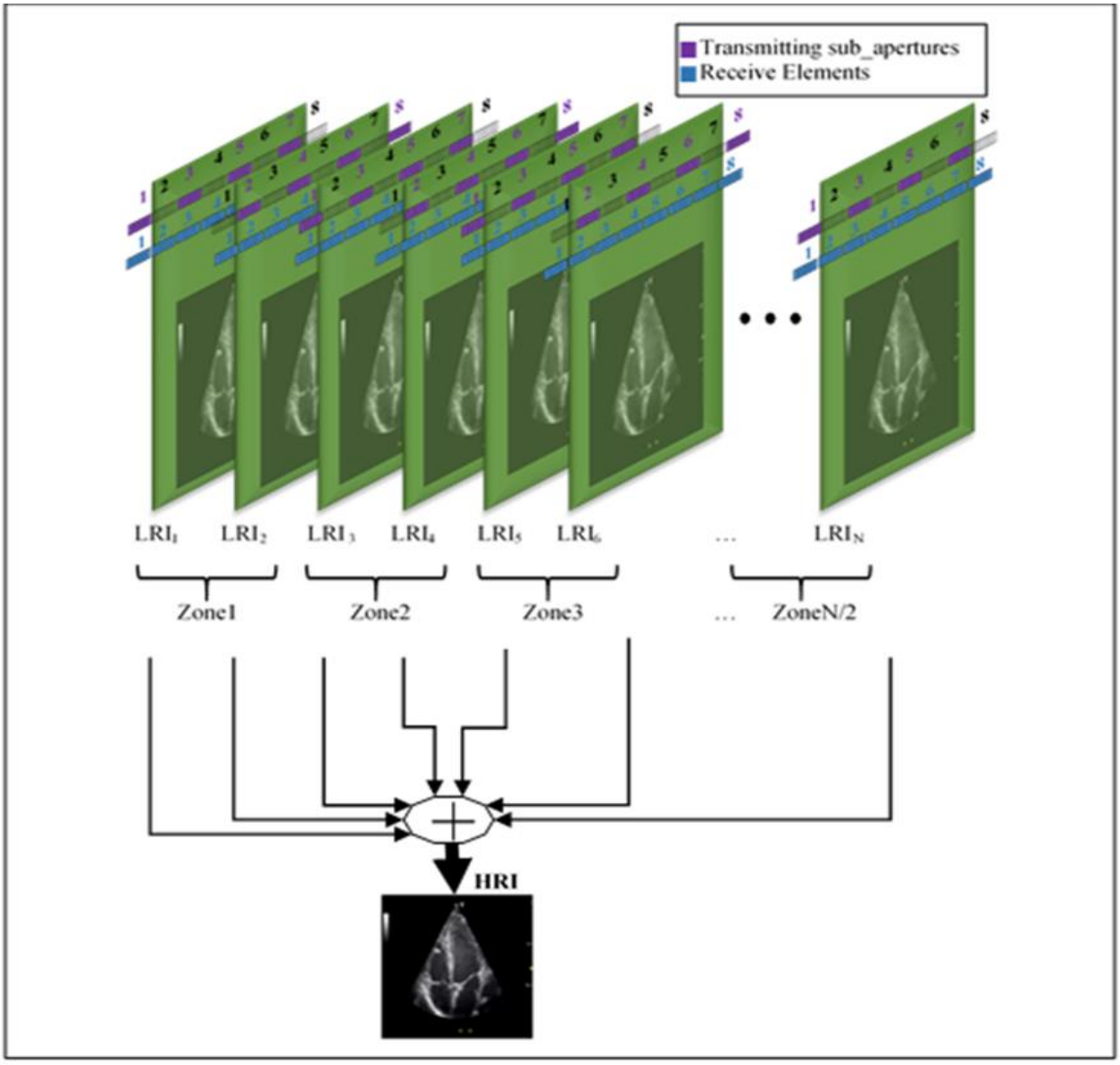

Fig. 11. High Resolution Image.

The insonification follows a certain firing order. For example, a focus point of Zone 1 and another in zone 5 are insonified at the same time. The same thing for a focus point of Zone 1 and another in zone 6 are insonified simultaneously.

Table I presents all the details about the focusing zones and the sub-apertures numbers and this is done for each emission number.

Here, zone 7 and zone 8 have one focusing point only. This decision is taken because the geometry surface spread over zones 7 and 8 is so small. So, we have decided here to gain frame rate. Also, we remark that (zone 2/zone 7+8), (zone 2/zone 6), (zone5/zone1) and (zone6/zone1) couples are highly spaced and echoes from these couples are temporally spaced. This makes the crosstalk highly reduced and maybe avoided between them. Here is the main idea of our new approach.

Another factor to talk about is the position of the focus centre for each transmission line per each transmission event. As you can deduce from the table below, the focusing point may be shared with multiple sub-apertures, here the position of the focusing point changes to be the centre of all the transmitting multi-elements' transducers. X1, X2,…X8 represent the fields that are perpendicular to the relative sub-apertures. For example, X1 is the field that is perpendicular to sub-aperture1, and so on to X8 which is perpendicular to sub-aperture 8. Fig. 13 and 14 describe the plotted emitted fields for each transmission synchronous line per each Low-resolution image.

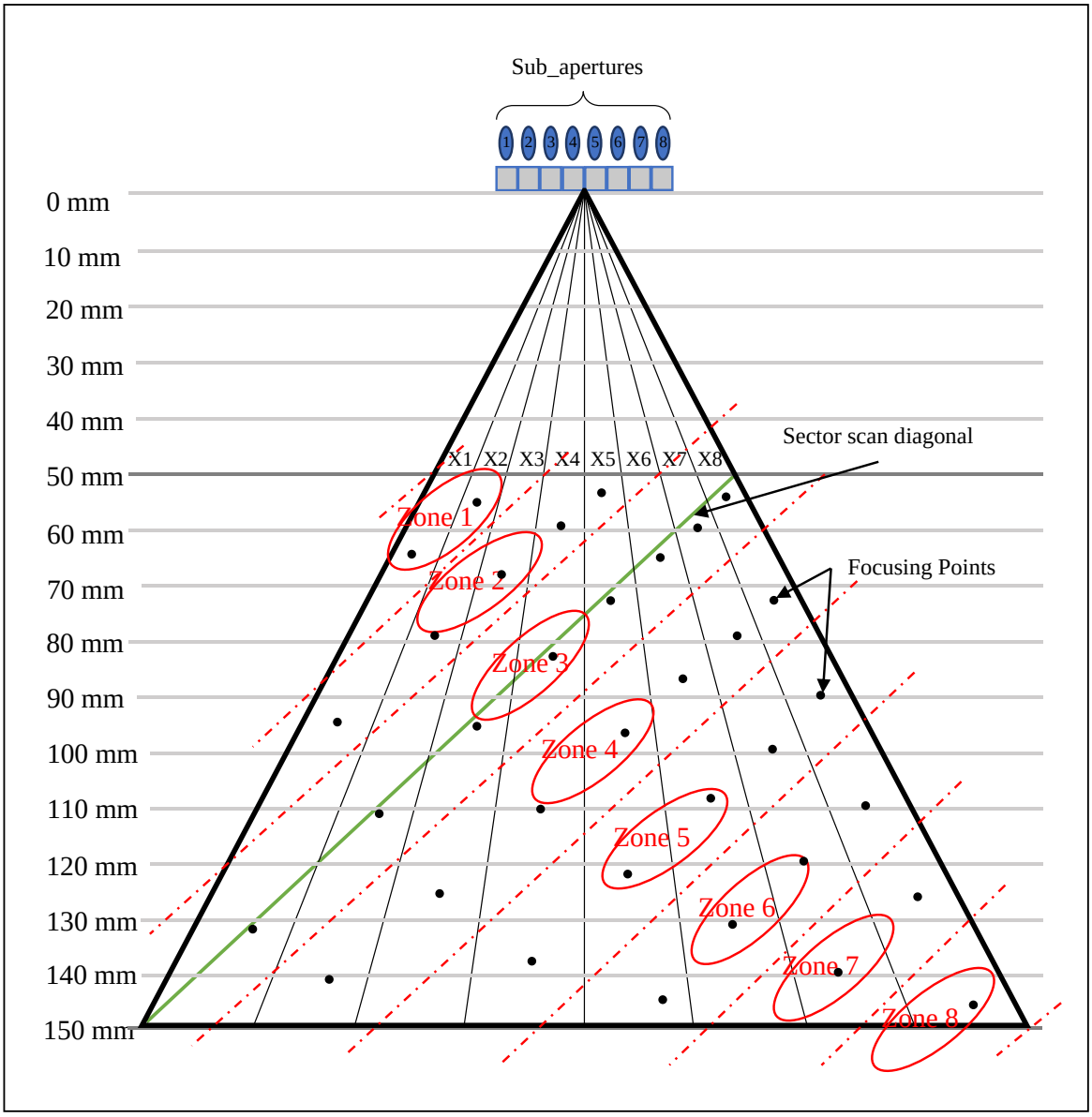

Fig. 12. Illustration of Synthetic Sum of Full MLT-MLA Scan Geometry (SSF-MLT-MLA-SG).

TABLE I. INSONIFICATIONS TABLE

Emission Number	**Focusing Zone Number**	**Sub_apertures (SbA)**							
		SbA 1	***SbA2***	***SbA 3***	***SbA 4***	***SbA 5***	***SbA 6***	***SbA7***	***SbA 8***
1	Zone2+7+8	95*X1	-	70*X3	-	55*X5	-	130*X8	
2	Zone 2 +6	80*X2		-	60*X4	-	130*X6	-	110*X8
3	Zone 3	130*X1	-	95*X3	-	75*X5	-	60*X7	
4	Zone 3	110*X2		-	85*X4	-	65*X6	-	55*X8
5	Zone 4	140*X2		-	110*X4	-	85*X6	-	75*X8
6	Zone 4	125*X3			-	95*X5	-	80*X7	
7	Zone 5	135*X4				-	110*X6	-	90*X8
8	Zone 5+1	55*X2		-	120*X5		-	100*X7	
9	Zone 6+1	65*X1		-	145*X5		-	120*X7	

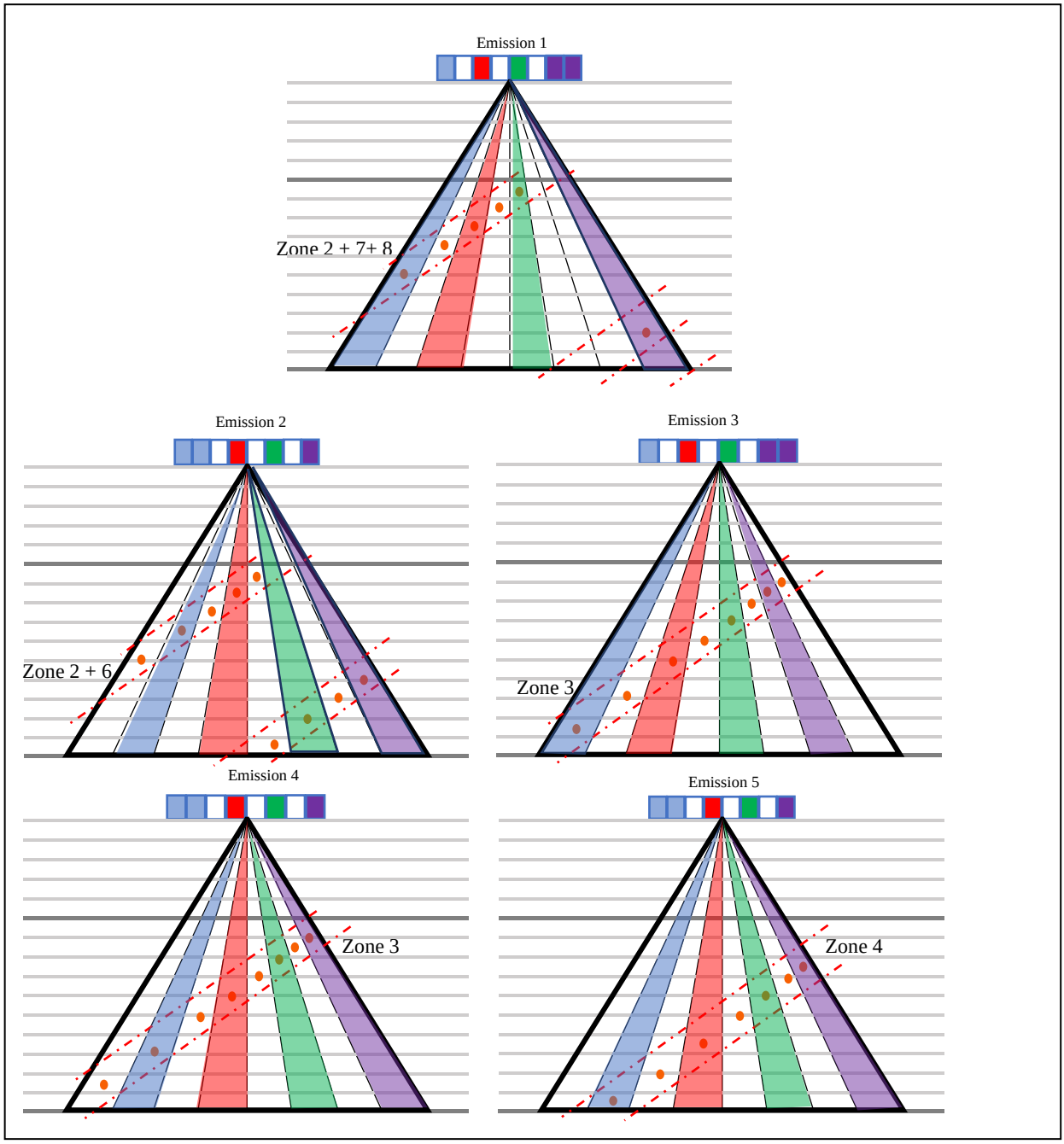

Fig. 13. Morphology of Focusing Point for each LRI: Emissions 1 to 5.

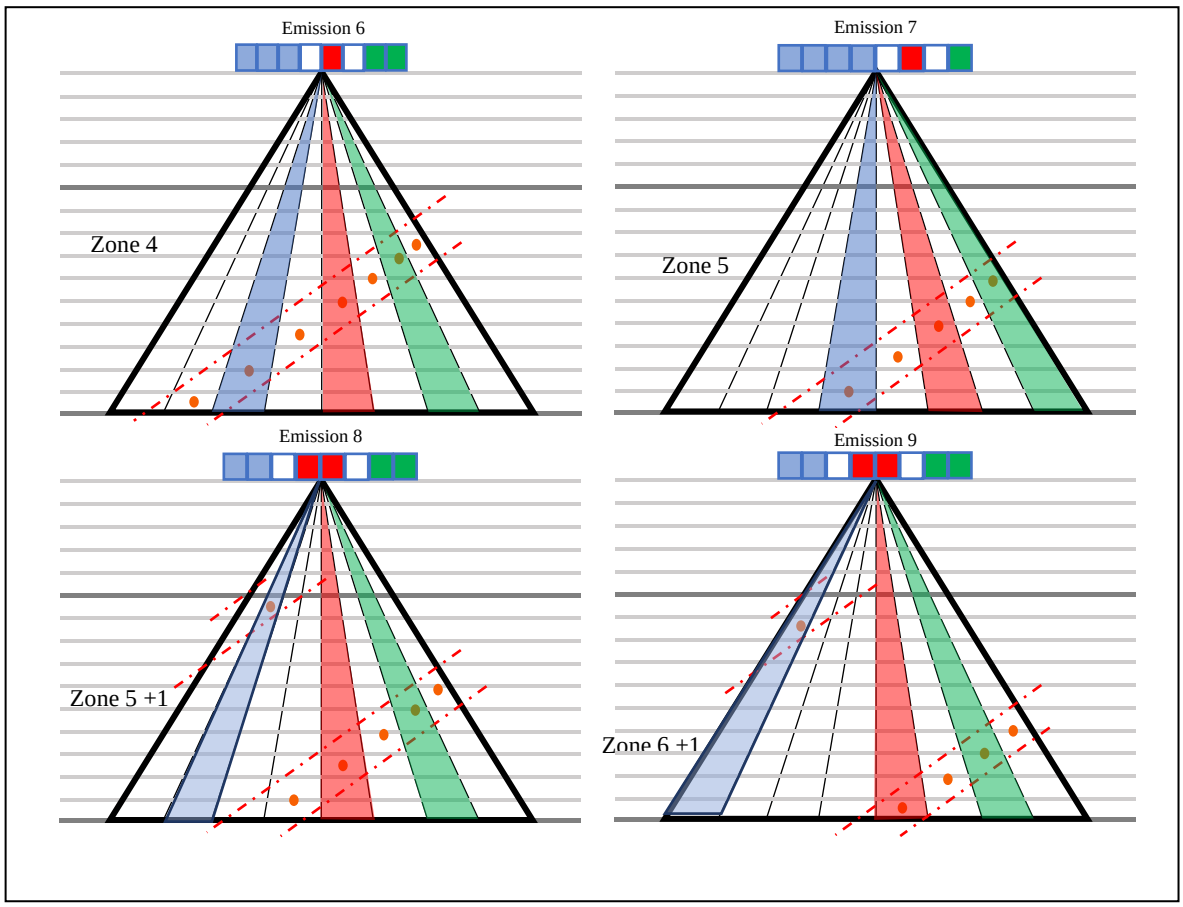

Fig. 14. Morphology of Focusing Point for each LRI: Emissions 6 to 9.

IV. Simulation Results

A. Simulation Setup

Each of the Point spread functions and the cyst phantoms are modelled. All the simulations are implemented in Matlab (MathWorks, Natick, Massachusetts) using Field_II. In the ultrasound software simulator [26], echo RF (Radio Frequency) data are produced using a 1D phased array transducer, which is composed of 128 elements with an element pitch of 193 μm and an element height of 5mm and an element width of 183 um and a kerf between adjacent elements of 10 um. This transducer is considered to scan a 30-image sectors using a speed of sound of 1540 m/s. Through transmission, the transducer generates a Hanning-windowed, 2-cycle sinusoid burst at 4 MHz and a relative bandwidth of 60% is used on transmission and the hanning apodization is applied accordingly. The same aperture with a hanning apodization is used in reception. The returned signals for each channel are sampled at 100 MHz. The RF data are imported to Matlab for beam forming. Dynamic reception focus is used for all the algorithms and the different beamforming techniques are applied to the recorded US signals. We use Hilbert transformation to the raw received RF data to detect the envelope and log compression. To prevent a coarse display due to a large image line spacing, we perform a low-pass interpolation to the raw received RF data laterally by a factor of 5. The scan conversion is in the last step to form the targetted image. All the images are represented over a 60-dB dynamic range.

B. Implemented Imaging Algorithms

To compare our proposed algorithm with the state-of-the-art 2-D cardiac imaging ones, subsequent beamforming methods are simulated. Their technical settings and detailed parameterization are described in the following paragraphs.

SLT in which the focusing points for each insonified beam are located at a penetration depth of 100 mm where all aperture elements are fired for each transmitting cycle. The focus points are equitably spread on a cylindrical shape centered at the middle of the transducer width, for a radius of 100 mm. The image lines are 128. Dynamic reception beamforming is exactly the mode used in this technique. Therefore, one transmission/reception event is employed to construct one scan line. Thus, for constructing one frame, one insonification is used line by line taking 26 milliseconds. So, the frame rate is approximately 40Hz (images per second).

8MLT beams are transmitted into 8 equidistant regions, each of them is splited into of 30/8 degrees opening angle. Focusing points are located at 100 mm depth for all parallel transmitting lines. After each insonification, 8 scan lines equal to the number of MLT beams are reconstructed simultaneously. To reconstruct an image of 128 lines, 16

firings are needed, and the resulting frame rate is 320frames per second (320 Hz).

16MLA beams are generated from 16 transmission events that focus on each time at the different regions, each of them is splitted into 30/8 degrees opening angle. Focusing points are located at 100 mm depth. After each insonification, 16 scan lines are reconstructed simultaneously. To generate an image of 128 lines, 8 firings are needed, and the resulting frame rate was 640frames per second (640 Hz). This imaging technique is simulated as a benchmark.

8MLT-16MLA beams are transmitted into 8 equidistant regions and 16 multilines are received. To reconstruct an image of 128 lines, 8MLT beams are transmitted into 8 equidistant regions, each of them is split into 30/8 degrees opening angle. Focusing points are located at 100 mm depth for all parallel transmitting lines. 16 MLA related to each region are reconstructed simultaneously around every transmission line, so 128 lines are generated for all MLT lines. Therefore, all scan lines forming one frame are generated simultaneously. Here we have a full image acquisition. One frame takes only one transmission/reception event, and the resulting frame rate is5128frames per second (5128 Hz).

In our algorithm, one High-resolution image is created after the Synthetic Sum of 9 low-resolution images. Every LRI is reconstructed with 128 MLA and a maximum with 4MLT beams that are transmitted into 4 equidistant azimuth planes with an inter-plane opening angle of 30/4 degrees. All MLT beams concerning each sub-aperture are focused at different depths, so, the first transmission line focuses on 70 mm and the second on 80 mm and so on and so forth to the last eighth line that focuses on 140 mm. The dynamic reception focus is adapted using the hole transducer elements to generate 128 MLA. For constructing one frame (HRI), we perform 9 transmission events equivalents to 9 LRI. The resulting frame rate is 5128/9frames per second (570 Hz).

C. PSF Results

The images of point spread are situated at 100 mm of depth obtained by SLT, 8_MLT, 16MLA, 8_MLT_16_MLAand SS-MLT beam formers are shown in Fig. 15, and the corresponding contour plots of the intensity point spread function is shown in Fig. 16. We can observe, in Fig. 15, that the SLT beam former exhibits the best performance and the best image quality output. We can notice in the same figure that 8_MLT beamformer shows approximately a performance that is a little bit better than our new proposed algorithm SS-MLT. After that, we remark that 16MLA occupies the fifth position concerning the image quality performance. Finally, we pay attention to 8_MLT_16_MLA algorithm that shows in the same figure also, the worst image quality. Fig. 16 is another form of displaying scan converted point spread function, so it exhibits the same analysis as the one described above.

Table II details the PSF performance for axial resolution. It shows the Full Width Half Maximum (FWHM), Full Width Half Dynamic Range (FWHDR), Main Lobe Width (MLW), Peak Side Lobe (PSL) and Double Main Lobe (DML) image quality options. The best parameters for each beamforming algorithm are highlighted in the table below. We notice that the best performances are obtained for the SS-MLT algorithm for which the values are respectively 58.6 for MLW, 82.6 for FWHM and 171.1 for FWDR. Similarly, SS-MLT has excellent values for PSL which is of the order of -503.609 as well as good values for DML which is of the order of -69.1 dB.

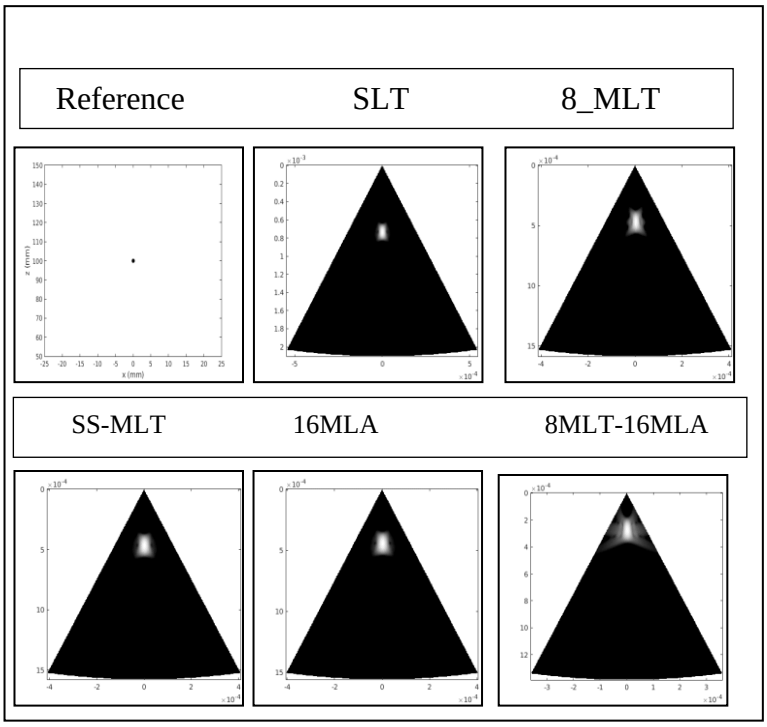

Fig. 15. PSF Results.

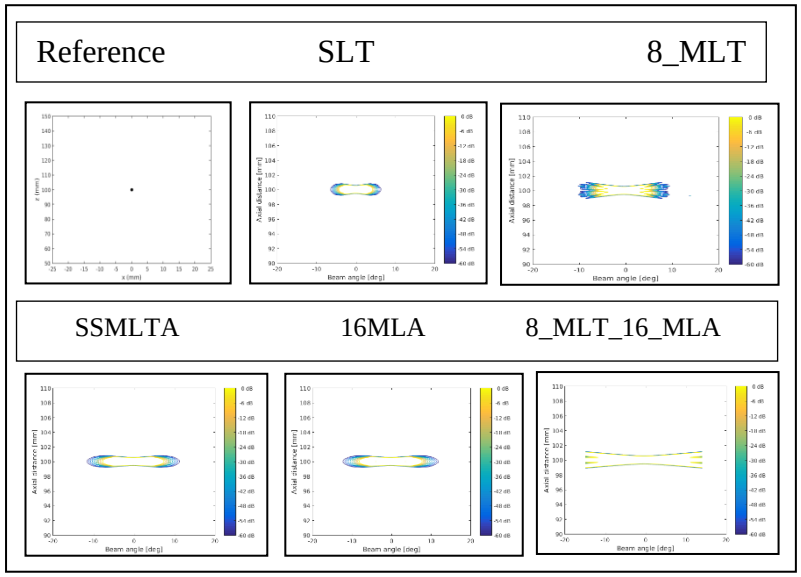

Fig. 16. PSF Contour Results

TABLE II. POINT SPREAD FUNCTION (AXIAL RESOLUTION)

Algorithm	MLW (μm)	FWHM (μm)	FWHDR (μm)	PSL (dB)	DML (dB)
SLT	**58.5**	**82**	**171**	**-550.511**	-68.6
8_MLT	**56.6**	**79.4**	**169.1**	-329.955	-67.9
SS-MLT	**58.6**	**82.6**	**171.1**	**-503.901**	**-69.1**
16MLA	58.6	82.8	171.3	**-498.884**	**-69.1**
8_MLT_16_MLA	59.3	83.3	171.9	-231.191	**-69.8**

In conclusion, SS-MLT has a very similar axial profile with the SLT, whose side lobes are almost always a little higher than those of the corresponding SLT, indicating a better image contrast resolution. The MLW for SS-MLT at a depth of 100 mm is less than that of the SLT, resulting in a wider FWHM and FWHDR than the SLT as shown in Table II.

Table III details the PSF performance metrics corresponding to the lateral resolution. Best MLW values are 57.6 µm, 44.4 µm, and, 66.8 µm for SLT, 8_MLT, and SS-MLT algorithms respectively. The best FWHM values are 82.8 µm, 55.3 µm, and 95.6 µm for SLT, 8_MLT, and SS-MLT algorithms respectively. Also, excellent FWHDR values are 184.5 µm, 97.1 µm, and 216.8 µm for SLT, 8_MLT, and SS-MLT algorithms respectively. The perfect PSL results are -378.469 dB, 0 dB, and -360.002 dB for SLT, 8_MLT, and SS-MLT algorithms respectively. The best DML results are -62 dB, -73.7 dB, and -60.2 dB for SLT, 8_MLT, and SS-MLT algorithms respectively.

This shows the same choices for image quality as axial resolution. Also illustrated are the optimal values of the three parameters for all techniques. SS-MLT showed a similar lateral profile with the SLT and 8-MLT, the PSL and DML of which are almost always marginally higher than that of the corresponding SLT and 8-MLT, suggesting an increased spatial resolution of the image contrast. The MLW for SS-MLT at a depth of 100 mm is a small greater than SLT and 8-MLT, resulting in a strong FWHM and FWHDR.

D. PSFs Results

The images of several point spread functions situated at different depths, in the [50mm-150 mm] range, obtained by SLT, 8_MLT, 16MLA, 8_MLT16_MLAand SS-MLT beamforming methods are shown in Fig. 17. We can remark that the similar image quality performance order like one point spread function could be noticed.

The efficiency metrics of PSFs compared to axial resolution are outlined in Table IV. For SLT, SS-MLT, and 8_MLT_16 MLA algorithms, the best MLW values are 59.6 mm, 58.9 mm, and 59.3 mm. The best FWHM values for SLT, SS-MLT, and 16MLA algorithms are 83.3 mm, 82.2 mm, and 83.2 mm respectively. Even for SLT, SS-MLT, and 16MLA algorithms, outstanding FWHDR values are 171.6 mm, 171.3 mm, and 172.2 mm respectively. For SS-MLT, 16MLA, and 8_MLT_16 MLA algorithms, the ideal PSL outcomes are -1,260 dB, -1,493 dB, and -1,412 dB, respectively. For SLT, SS-MLT, and 8 MLT 16 MLA algorithms, the best DML results are -69.8 dB, -69.1 dB, and -69.5 dB.

TABLE III. POINT SPREAD FUNCTION (LATERAL RESOLUTION)

Algorithm	*MLW (µm)*	*FWHM (µm)*	*FWHDR (µm)*	*PSL (dB)*	*DML (dB)*
SLT	**57.6**	**82.8**	**184.5**	**-378.469**	**-62**
8_MLT	**44.4**	**55.3**	**97.1**	**-7.3896e-13**	**-73.7**
SS-MLT	**66.8**	**95.6**	**216.8**	**-360.002**	**-60.2**
16MLA	84.1	120.3	272.2	-356.123	-59.7
8_MLT_16_MLA	94.9	134.9	305.3	-128.235	-59.8

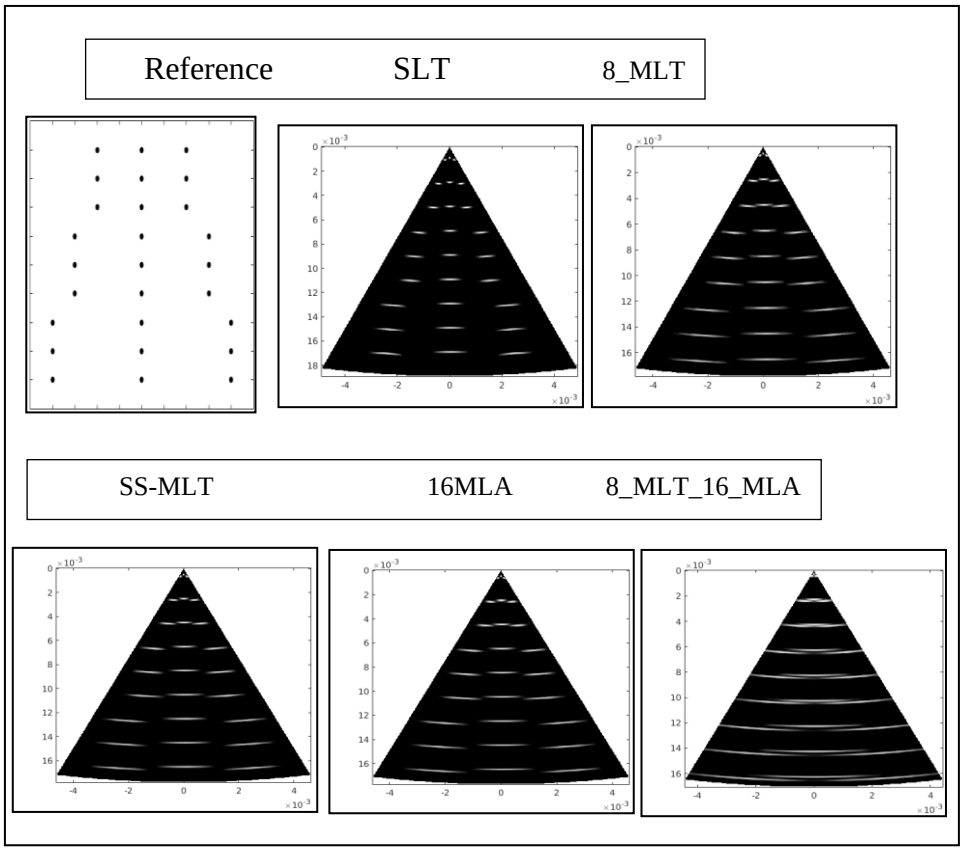

Fig. 17. PSFs Results.

TABLE IV. POINT SPREAD FUNCTIONS (AXIAL RESOLUTION)

Algorithm	*MLW (µm)*	*FWHM (µm)*	*FWHDR (µm)*	*PSL (dB)*	*DML (dB)*
SLT	**59.6**	**83.3**	**171.6**	-0.535	**-69.8**
8_MLT	59.8	84.3	174.6	-0.312	-68.8
SS-MLT	**58.9**	**83.2**	**171.3**	**-1.260**	**-69.1**
16MLA	59.7	**82.2**	**172.2**	**-1.493**	-68.5
8_MLT_16_MLA	**59.3**	83.5	172.7	**-1.412**	**-69.5**

Table V details the performance metrics of PSFs relative to lateral resolution. The best MLW values are 32.5 mm, 72.7 mm, and 59.9 mm for the 8-MLT, SS-MLT, and 8_MLT_16_MLA algorithms. The highest FWHM values are 49.5 mm, 102.9 mm, and 130 mm for the 8 MLT, SS-MLT and 16MLA algorithms, respectively. Excellent FWHDR values are 133 mm, 227.6 mm and 186.7 mm also for 8-MLT, SS-MLT and 16MLA algorithms. For 16MLA, SS-MLT, and 8_MLT_16_MLA algorithms, the optimal PSL outcomes are -1,260 dB, -1,493 dB, and -1,412 dB. For SLT, SS-MLT, and 8_MLT_16_MLA algorithms, the best DML results are -63.5 dB, -60.1 dB, and -60.4 dB, respectively.

TABLE V. POINT SPREAD FUNCTIONS (LATERAL RESOLUTION)

Algorithm	*MLW (μm)*	*FWHM (μm)*	*FWHDR (μm)*	*PSL (dB)*	*DML (dB)*
SLT	131	185.5	404.3	-0.535	**-63.5**
8_MLT	**32.5**	**49.5**	**133**	-0.312	-51.3
SS-MLT	**72.7**	**102.9**	**227.6**	**-1.493**	**-60.1**
16MLA	92.6	**130**	289.8	**-1.260**	-59.2
8_MLT_16_MLA	**59.9**	85	**186.7**	**-1.412**	**-60.4**

E. Cyst Phantom (CP) Results

Ten cysts with a radius that varies from 8.5mm to 2 mm are located at five depths of imaging to evaluate the beamformers under the cyst targets. The cyst phantom consists of a collection of point targets, five cyst regions, and five highly scattering regions. This can be used for characterizing the contrast-lesion detection capabilities of an imaging system. The scatterers in the phantom are generated by finding their random position within a 100 x 100 x 10 mm cube, and then ascribe a distributed Gaussian amplitude to each scatterer. If the scatterer resides within a cyst region, the amplitude is set to zero. Within the highly scattering region, the amplitude is multiplied by 20. The phantoms typically consist of 200,000 scatterers and simulating to 128 RF lines.

The reconstructed images are provided in Fig. 18. As it can be seen, the cyst targets are not well detected in the image generated by 8_MLT_16_MLA. Moreover, the reconstructed images are defected by the effects of the noise. Even though SS-MLT results in a higher-quality image and more detectable cyst targets, in comparison with 16MLA, the effects of the produced noise are still obvious. Besides, SLT suppresses the effects of the noise further, as was illustrated for wire targets, and results in a higher image quality in addition to8_MLT.

The PSNR, SNR and CPP parameters are determined for the reconstructed images for a quantitative analysis. The previous efficiency metrics for each cyst-using beamformer are listed in Table VI. For 8_MLT_16_MLA, 8 MLT, and SS-MLT algorithms, the best SNR values are 16.34 dB, 17.29 dB, and 16.90 dB. For 8_MLT_16_MLA, SS-MLT, and 16MLA algorithms, the optimal PSNR results are -29.91 dB, -30.46 dB, and -30.42 dB. We used SLT as a reference algorithm, to study the SNR and the PSNR for the other methods. The greatest CNR values are 54.24 dB, 54.70 dB, and, 54.15 dB for SLT, 8_MLT_16_MLA, and SS-MLT algorithms, respectively. Also, the best CPP values are 25.06 dB, 25.45 dB, and, 25.09 dB for SLT, 8-MLT, and 16MLA algorithms, respectively.

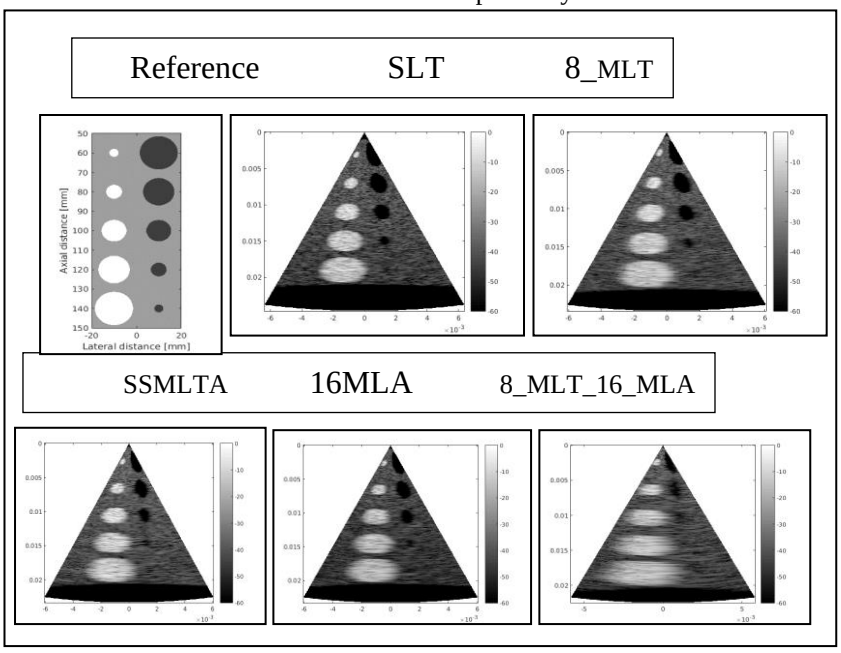

Fig. 18. Cyst_Phantom Results (200000 Scatterers).

TABLE VI. PERFORMANCE METRICS OF CYST PHANTOM

Algorithms	*SNR (dB)*	*PSNR (dB)*	*CNR (dB)*	*CPP*
SLT	Reference*	Reference*	**54.24**	**25.06**
8_MLT	**17.29**	-29.40	52.83	**25.45**
SS-MLT	**16.90**	**-30.46**	**54.15**	25.54
16MLA	16.22	**-30.42**	53.77	**25.09**
8_MLT_16_MLA	**16.34**	**-29.91**	**54.70**	25.74

*:SLT algorithm is taking as reference in comparison with other algorithms.

V. DISCUSSION

In this study, we brought to the fore a new implementation technique for a 2-D MLT system. As the MLT methods suffer from the crosstalk artifacts, we introduced many developments and enhancements in order to reduce the negative impact of these problems. Synthetic Sum of full MultiLine Transmission (SS-MLT) low-resolution images focused at diagonal focusing depths is our new proposed modality which allows for an improved image quality in 2D echocardiography imaging applications. Taking advantage of the diagonal synchronous focusing points, we highly decrease the interference among the different transmission/reception beams of the images and therefore reduce the amplitude of the crosstalk artifacts. Using sparse transmitting sub-apertures, we avoided transmission side-lobe/side-lobe beams interference between adjacent transmitted beams. Also, windowing functions adopted with the sub-aperture elements for both transmission and events might reduce the main-lobe/side-lobe interactions and equivalently reduce the transmission/reception crosstalk levels. In this work, we used Hanning apodization on transmission and on reception, which gives further perfections and improvements in the decreasing of the crosstalk artifacts for all simulations.

Simulation results prove that our new proposed method is effective and promising regarding point spread function performances, thus it competes for SLT image quality options for many configurations. Besides, for cyst phantom simulations, it has shown good CNR and SNR and this is done to the low crosstalk levels as we explained above. Table VII gives an approximative order of the algorithms referring to their operating frame rate and their image quality performances. Although the SS-MLT runs at a higher frame rate than 8MLT, it exhibits better competences than those of B-mode images.

TABLE VII. FRAME RATE AND IMAGE QUALITY BEST ORDER

Best Image Quality per Order	*Algorithm*	*Frame Rate (Hz)*
1	SLT	5128/128
3	8_MLT	5128/16
2	SS-MLT	5128/9
4	16MLA	5128/8
5	8MLT-16MLA	5128

VI. CONCLUSION

This paper demonstrates a new MLT-MLA technique that benefits from the shape of the sector scan geometry. We suggest distributing multiple focusing points along the diagonal of the sector scan geometry. The synthetic sum of multiple low-resolution images is adopted to bring a higher resolution image. Each LRI is constructed with MLT lines. By using sparse sub_apertures, the interference is reduced and by using different focusing depths the spatial resolution of the images is ameliorated with a good SNR and CNR and perfect FWHM lateral resolution and axial resolution values. Adequately, the crosstalk noise is drastically reduced while maintaining a high frame rate that allows 2D echocardiography imaging. After we have accurately studied all the conditions of implementation of our method, and after we concluded that it was very promising for cardiac applications, we concentrate now on its hardware implementation to further evaluate its reliability and effectiveness.

REFERENCES

[1] T. Szabo, Diagnostic Ultrasound Imaging—Inside Out. 2004.

[2] M. Cikes, L. Tong, G. R. Sutherland, and J. D'hooge, "Ultrafast cardiac ultrasound imaging: technical principles, applications, and clinical benefits," JACC: Cardiovascular Imaging, vol. 7, pp. 812-823, 2014.

[3] H. Chen, T. Varghese, P. S. Rahko, and J. A. Zagzebski, "Ultrasound frame rate requirements for cardiac elastography: Experimental and in vivo results," Ultrasonics, vol. 49, no. 1, pp. 98–111, Jan. 2009.

[4] H. Hasegawa, H. Kanai., "High-frame-rate echocardiography using diverging transmit beams and parallel receive beamforming," J. Med. Ultrason, Vol. 38, pp. 129–140, Jul. 2001.

[5] L. Tong et al., "Comparison of Conventional Parallel Beamforming With Plane Wave and Diverging Wave Imaging for Cardiac Applications: A Simulation Study," IEEE Trans. Ultrason. Ferr. Freq. Control, Vol. 59, pp. 1654–1663. 2012.

[6] Ø. Ragnhild. "Coherent Plane-Wave Compounding in Medical Ultrasound Imaging: Quality Investigation of 2D B-mode Images of Stationary and Moving Objects," 2012.

[7] T. Shirasaka, "Ultrasonic imaging apparatus," US Patent 4815043, Mar. 1989.

[8] L. Tong, H. Gao, and J. D'hooge "Multi-transmit beam forming for fast cardiac imaging: quantitative analysis of the cross-talk between MLT beams," IEEE International Ultrasonics Symposium, Dresden, Germany, pp. 1271–1274, 2012.

[9] L. Tong, A. Ramalli, R. Jasaityte, P. Tortoli, and J. D'hooge, "Multitransmit beam forming for fast cardiac imaging–experimental validation and in vivo application," IEEE Trans. Med. Imag., vol. 33, no. 6, pp. 1205–1219, Jun. 2014.

[10] L. Demi et al., "Implementation of Parallel Transmit Beamforming Using Orthogonal Division Multiplexing—Achievable Resolution and Interbeam Interference," IEEE Trans. Ultrason. Ferroelectr. Freq. Control., Vol. 60, pp. 2310–2320, 2013.

[11] L. Demi et al., "Tissue harmonic images obtained with parallel transmit beamforming by means of orthogonal frequency division multiplexing," In Proceedings of the 2014 IEEE International Ultrasonics Symposium (IUS)., 3-6 September 2014, Chicago, Illinois pp. 1213-1216, Sep. 2014.

[12] B. Denarie, H. Torp, T. Bjastad, "A Novel Approach for Reducing Multi Line Transmission Cross-talks using 2D Transducer Arrays," IEEE International Ultrasonics Symposium, Dresden, Germany, pp. 2242 – 2245, 2012.

[13] B. Denarie, T. Bjastad, and H. Torp, "Multi-line transmission in 3-D with reduced crosstalk artifacts: A proof of concept study," IEEE Trans. Ultrason. Ferroelectr. Freq. Control, vol. 60, no. 8, pp. 1708–1718, 2013.

[14] A. Ramalli, L. Tong, J. Luo, J. D'hooge, P. Tortoli, "Safety of fast cardiac imaging using multiple transmit beams: experimental verfication," UltrasonicsSymp. (IUS), 2014 IEEE International, 2014.

[15] A. Ramalli et al., "Real-Time High-Frame-Rate Cardiac B-Mode and Tissue Doppler Imaging Based on Multiline Transmission and Multiline Acquisition," IEEE Trans. Ultrason. Ferroelectr. Freq. Control, vol. 65, no. 11, pp. 2030–2041, Nov. 2018.

[16] P. Santos, L. Tong, A. Ortega, EigilSamset, and J. D'hooge, "Safety of Multi-line transmit beam forming for fast cardiac imaging – a simulation study," UltrasonicsSymp. (IUS), 2014 IEEE International, 2014.

[17] L. Tong et al., "Fast three-dimensional ultrasound cardiac imaging using multi-transmit beamforming: A simulation study," IEEE Ultrason. Symp. Proc., Vol. 60, pp. 1456–1459, 2013.

[18] L. Tong, H. Gao, and J. D'hooge, "Multi-transmit beam forming for fast cardiac imaging-a simulation study," IEEE Trans. Ultrason. Ferroelectr. Freq. Control, vol. 60, no. 8, pp. 1719– 1731, Aug. 2013.

[19] L. Demi, M. D. Verweij, and K. W. A. Van Dongen, "Parallel transmit beamforming using orthogonal frequency division multiplexing applied to harmonic Imaging-A feasibility study," IEEE Trans. Ultrason. Ferroelectr. Freq. Control, vol. 59, no. 11, pp. 2439–47, Nov. 2012.

[20] D. Dubberstein and O. V. Ramm, "Methods and systems for ultrasound scanning using spatially and spectrally separated transmit ultrasound beams," U.S. Patent 6159153, Dec. 12, 2000.

[21] K. Thiele, "Multi-beam transmit isolation," U.S. Patent 20100016725, Jan 21, 2010.

[22] J. Hossack and T. Sumanaweera, "Method and apparatus for medical diagnostic ultrasound real-time 3-D transmitting and imaging," U.S. Patent 6179780, Jan. 30, 2001.

[23] C. Yoon, et al.,"Orthogonal quadratic chirp signals for simultaneous multi-zone focusing in medical ultrasound imaging." IEEE Trans. Ultrason. Ferroelectr. Freq. Control, vol 59, pp. 1061–1069, 2012.

[24] F. Prieur, B. Dénarié, A. Austeng, and H. Torp, "Correspondence—Multi-line transmission in medical imaging using the second-harmonic signal," IEEE Trans. Ultrason., Ferroelectr., Freq. Control, vol. 60, no. 12, pp. 2682–2692, Dec. 2013.

[25] L. Tong et al., "Coded excitation for crosstalk suppression in multi-line transmit beamforming: Simulation study and experimental validation," Appl. Sci., vol. 9, no. 3, p. 486, Jan. 2019.

[26] J.A. Jensen., "Field: a program for simulating ultrasound systems,"10th Nordicbaltic conference on biomedical imaging., pp. 351-353, 1996.